JOURNAL OF AIRCRAFT
Vol. 31, No. 4, July–Aug. 1994

Jet Ground Vortex Formation by Annular Jets

John M. Kuhlman* and William M. Cavage†
West Virginia University, Morgantown, West Virginia 26506

An experimental study has been conducted of the impingement of a single circular jet on a ground plane in a crossflow. This geometry is a simplified model of the interaction of propulsive jet exhaust from a V/STOL aircraft with the ground in forward flight. Jets have been oriented normal to the crossflow and ground plane. Jet size, crossflow-to-jet velocity ratio, ground plane-to-jet board spacing, jet exit turbulence level, and mean velocity profile shape have all been varied to determine their effects on the size of the ground vortex interaction region which forms on the ground plane, using smoke injection into the jet. Variation of observed ground vortex size with crossflow-to-jet velocity ratio was consistent with previous studies. Observed effects of jet size and ground plane-to-jet board spacing were relatively small. Jet exit turbulence level effects were also small. However, an annular jet with a low velocity central core was found to have a significantly smaller ground vortex than an equivalent uniform jet at the same values of crossflow-to-jet velocity ratio and jet exit-to-ground plane spacing. This may suggest a means of altering ground vortex behavior somewhat, and points out the importance of proper simulation of jet exit velocity conditions. Laser velocimeter data indicated unsteady turbulence levels in the ground vortex as high as 80%.

Nomenclature

A_e = effective jet exit area
D = nozzle diameter
D_e = effective jet exit diameter
h = spacing between jet nozzle exit and ground plane
K = jet kinematic momentum flux
MF = jet exit momentum flux
$\dot{m}$ = jet initial mass flux
p = jet exit static pressure
p_{noz} = jet nozzle inlet static pressure
Q = jet initial volume flux
q_{max} = maximum jet exit dynamic pressure
R = gas constant
T = jet stagnation temperature
u = jet axial velocity
V_e, V_j = effective jet exit velocity
V_{max} = measured maximum jet exit velocity
V_∞ = crossflow velocity
x = coordinate direction along crossflow direction
x_p = maximum upstream penetration of ground vortex
y = spanwise coordinate direction
Z_b = spacing between jet board and ground plane
z = coordinate direction along jet axis
γ = specific heat ratio
ρ = jet exit density

Introduction

WHEN a circular jet impinges nearly normal to a ground plane, a radial wall jet is formed. If the jet interacts with the ground plane in the presence of a weak crossflow ($V_\infty/V_j << 1$) moving parallel to the ground, then as the radial wall jet slows, the upstream portion of the wall jet separates from the wall and turns back on itself to form an unsteady, recirculating vortex flow termed the ground vortex. This flow is qualitatively similar to the horseshoe or "necklace" vortices formed around bridge piers, etc., but is in fact highly unsteady and much less organized. This ground vortex can have adverse aerodynamic effects on the performance of a V/STOL aircraft in close proximity to the ground.

The area of propulsion-induced aerodynamic effects out of ground effect has received a great deal of interest, as summarized by Margason.[1,2] Kuhn[3] and Stewart[4] have focused on reviewing prior aeropropulsion interaction work in ground effect; typical studies of ground effects are those due to Abbott,[5] Hall,[6] Colin and Olivari,[7] and Hall and Rogers.[8]

Because of its simplicity, the interaction of a single jet issuing from a flat plate into a crossflow has also received a great deal of attention as a model problem capturing much of the basic physics. Margason[9] measured jet centerline trajectories out of ground effect for a range of jet-to-crossflow velocity ratios and jet injection angles. Ziegler and Wooler[10] studied a series of uniform and nonuniform jets issuing into a crossflow out of ground effect, and developed the concept of an equivalent, uniform jet of equal thrust and initial mass flux, to allow comparisons of trajectory and jet-induced pressures around the jet exit for the various nonuniform jets. Chassaing et al.[11] measured detailed mean velocity distributions for a series of circular and annular jets interacting with a crossflow. Kuhlman and Warcup[12] and Kuhlman et al.[13,14] also studied the annular jet in a crossflow, and found a significant decrease in the jet-induced lift loss as the jet decay rate was increased.

The circular jet in hover out of ground effect was studied by Gentry and Margason,[15] and Kuhlman and Warcup.[16,17] Again, jet decay rate was found to influence the jet-induced lift loss, but in hover quicker jet decay increased the lift loss. Kuhlman[18] clearly showed this to be due to the increased entrainment into the jet when jet centerline velocity decay rate was increased. Kuhlman and Gross[19,20] have recently documented the three-dimensional mean and turbulence characteristics of the circular jet without crossflow using the three-component laser velocimeter (LV) which has been used in the present study.

Recent experimental studies of a circular jet in a confined crossflow include work by Catalano et al.,[21] Chen and Hwang,[22] Barata et al.,[23] and Barata.[24] The interaction of a circular jet with a confined crossflow, and impingement with the opposite crossflow channel walls, has been documented in each of these studies using LV. However, although some evidence of the formation of a ground vortex ahead of the impingement points

Presented as Paper 92-4251 at the AIAA Aircraft Design Systems Meeting, Hilton Head, SC, Aug. 24–26, 1992; received Sept. 20, 1992; revision received April 21, 1993; accepted for publication July 24, 1993.

*Professor, Mechanical and Aerospace Engineering Department. Associate Fellow AIAA.

†Graduate Research Assistant, Mechanical and Aerospace Engineering Department. Student Member AIAA.

of some of these jets was observed, the behavior of the ground vortex was not documented in detail.

More detailed experimental investigations of ground vortex formation include Cimbala, et al.,[25,26] Billet and Cimbala,[27] Paulson and Kemmerly,[28] Kemmerly and Paulson,[29] and Stewart.[30] Cimbala et al. studied the effects of crossflow-to-jet velocity ratio, approach boundary-layer thickness, and jet exit-to-ground board spacing, on the size of the ground vortex using flow visualization, laser velocimetry, and centerline static pressures on the ground board. Spectral data were used to characterize the unsteady nature of the ground vortex. Stewart focused on the effects of a moving jet vs a stationary jet in a wind tunnel, whereas Paulson and Kemmerly studied the effects of sink rate on ground vortex formation. Computational efforts include Van Dalsem and Steger,[31] Van Dalsem et al.,[32] and Smith et al.[33] Navier-Stokes CFD simulations have been obtained for circular and elliptical, laminar and turbulent jets in a crossflow impinging on a ground plane, with generally good agreement with experimentally observed ground vortex location. The recent work of Smith et al. presents a simulation of the flow around the complete Harrier AV-8B configuration in ground effect.

The current study is similar to the work of Cimbala et al.,[25,26] but focuses on the feasibility of using nonuniform jet exit velocity distributions, in the form of an annular jet with a low velocity core, to reduce the size of the ground vortex interaction region. In addition, the effects of jet Reynolds number and tunnel sidewall location, jet exit turbulence level, and confinement of the flow between the ground plane and a jet board through which the jet exhausts, have been investigated. The present work has been described in greater detail by Cavage.[34]

Experimental Facility and Procedures

Experiments have been conducted in the low-speed wind tunnel at West Virginia University. The tunnel is a closed return, atmospheric facility with a test section 0.813 × 1.14 m (32 × 45 in.) in cross section by 1.22 m (48 in.) in length. Maximum test section crossflow velocity is about 76 m/s (250 ft/s) with no turbulence screens installed. The present experiments have been conducted with one turbulence screen installed in the plenum; the test section nozzle is formed from a 6:1 area ratio rectangular contraction.

The jet-ground vortex facility used in the present work has been shown schematically as viewed from above in Fig. 1. The jet flow is created by a variable speed blower, and flows across the tunnel test section via a 10-cm- (4-in.-) diam acrylic tube to a machined aluminum jet nozzle. A flow straightener made from plastic drinking straws and screens is installed in the acrylic tube. The jet exits through a 1.3-cm- (0.5-in.-) thick acrylic jet board which is parallel to the 0.48-cm- (0.187-in.-) thick glass side wall of the tunnel test section, which serves as the ground plane and provides optical access for both the flow visualization and LV measurements. The spacing between the jet board and the ground plane is continuously adjustable from 8 cm (3 in.) to 23 cm (9 in.), which allows variation of h.

A series of interchangeable jet nozzles have been used, having three different jet exit diameters of D = 0.95, 1.27, and 2.54 cm (0.375, 0.50, and 1.0 in.), as shown in Fig. 2. Most results have been obtained using the D = 1.27-cm (0.5-in.) nozzle, at an exit velocity of 91.4 m/s (300 ft/s). Nozzle contours have been designed to be smooth by using a 12.7-cm- (5-in.-) radius circular arc curvature for the upstream portion of the nozzle, with appropriate opposite-signed circular arc curvatures used in the downstream portion of the nozzles to yield the desired exit diameter. The two circular arc portions are tangent to one another at the transition point, but with a jump in curvature. In addition, the exit lips of all jet nozzles protrude beyond the plane of the jet board. Most nozzles have an exit lip which extends $2D$ beyond the jet board, as shown in Fig. 2, although nozzles which extend 4, 7, and $13D$ have also been used in a study of the confining effect of the jet board on ground vortex size. These nozzles have overall area ratio contractions of 114, 64, and 16:1, for the 0.95-, 1.27-, and 2.54-cm-diam jets, respectively.

Two special nozzles have also been used, both having exit diameters of D = 1.27 cm (0.5 in.), and extending $2D$ beyond the jet board. The first has a turbulence generating plate installed at the tangency point where the nozzle curvature changes sign. The aluminum turbulence generating plate has 0.476-cm (0.188-in.) holes on staggered 0.635-cm (0.25-in.) centers, yielding a solidity of 0.5.

The second special nozzle has a 0.952-cm (0.375-in.), or $0.75D$ diam cylindrical centerbody mounted concentrically in the nozzle and submerged $0.5D$ beneath the jet exit plane, as shown in Fig. 3. This centerbody has a hemispherical tip. This configuration generates a high-velocity annular jet with a low velocity central core region. It is this configuration which Kuhlman[18] demonstrated to have dramatic increases in both near-field and far-field entrainment, relative to an equivalent uniform velocity, low exit turbulence level circular jet of equal momentum flux, and initial mass flux.

Jet exit velocity profiles have been measured using a traversable 1.6-mm- (1/16-in.-) diam pitot-static probe and micromanometer; measured velocity profiles have been integrated numerically to calculate momentum flux and initial volume flow rate Q for each nozzle. Traverses were performed in two orthogonal directions to ensure symmetry of the flow. Examples of the measured jet exit velocity profiles have been presented in Figs. 4 and 5, for the standard jet and annular

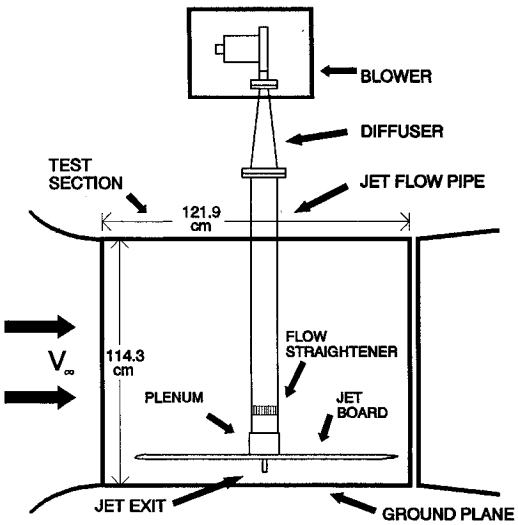

Fig. 1 Schematic of ground vortex jet facility viewed from above.

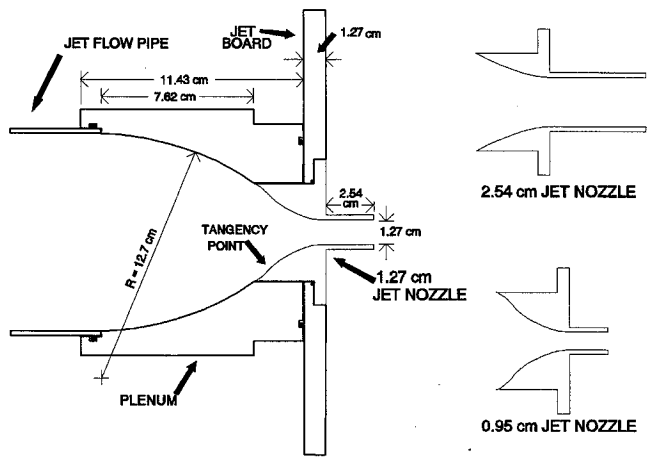

Fig. 2 Cross section of jet nozzles and plenum.

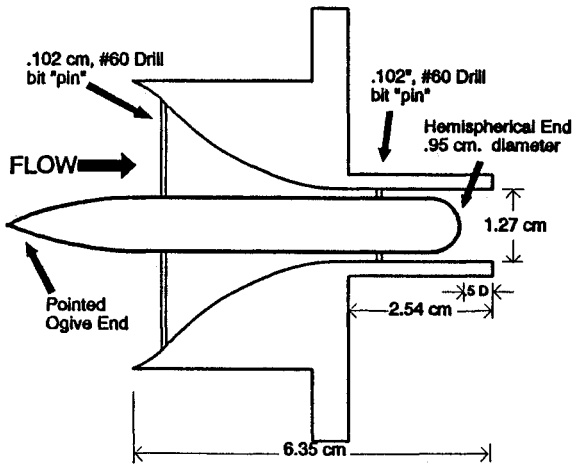

Fig. 3 Cross section of annular jet nozzle fitted with hemispherical tip centerbody.

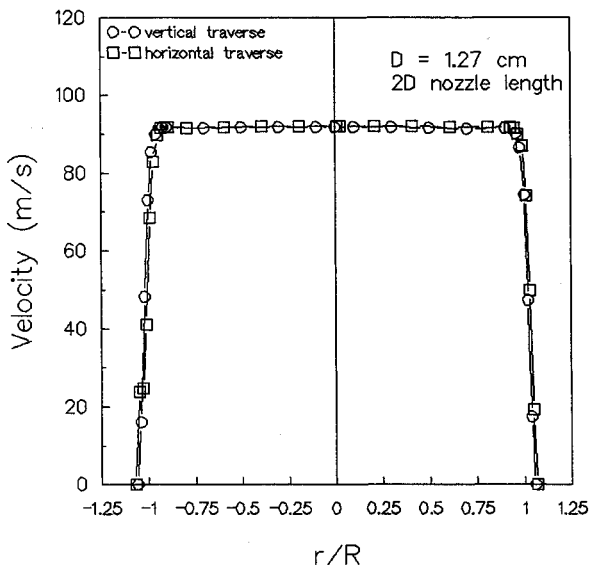

Fig. 4 Typical nozzle exit mean velocity traverses for 1.27-cm-diam nozzle.

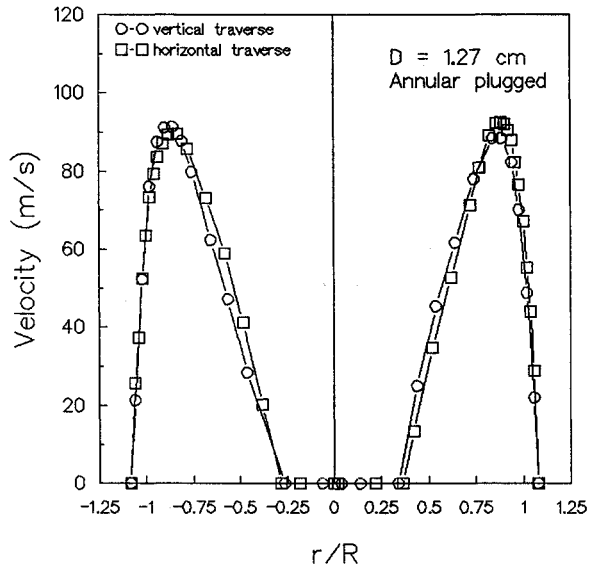

Fig. 5 Typical nozzle exit mean velocity traverses for 1.27-cm-diam annular nozzle.

jet, respectively. Nonzero velocities measured beyond the jet exit radius are due to the size of the pitot probe, and have been ignored in this integration process. The finite size of the stagnation pressure orifice causes a smearing of the velocities in the shear layer. The calculated Q values have been compared with volume flow rates for ideal "top hat" velocity profiles to obtain nozzle discharge coefficients for all nozzles except the annular jet nozzle; these discharge coefficients range from approximately 0.98–0.99 (see Table 1). Once each nozzle had been calibrated in this fashion, the jet exit velocity has been set by setting the value of the static pressure measured just upstream of the converging jet nozzle; accuracy of the resulting jet velocity is estimated to be approximately 1% based upon repeatability of the data.

Flow visualization studies have been conducted using smoke generated by a commercial fog machine; the smoke has been injected into the jet through the blower inlet. Videotape as well as 35-mm slide film has been used to record images of the smoke in the jet and the ground vortex, as viewed along the jet axis through the glass ground board under room light. A grid of 2.54-cm (1-in.) squares has been drawn on the ground board to enable quantitative determination of both the size of the ground vortex and jet impingement location. In addition, laser light sheet flow visualization has been used. Flowfield cuts perpendicular to the crossflow at various axial stations and on the symmetry plane have been illuminated by a sheet of laser light generated by the Argon ion laser used for the laser velocimeter system and a cylindrical lens. Again, smoke was injected into the jet and the shape of the ground vortex at various crossflow stations was recorded on videotape and slide film.

Velocity measurements in the ground vortex have been made using a three-component, five-beam commercial DANTEC system similar to one described by Buchave.[35] This LV system has been used previously[19,20] to measure three-dimensional velocities in a circular air jet. Independent two-channel and one-channel LV optics make up the nonorthogonal three-component system. Results have been computed using standard statistical averaging, omitting spurious outlier data.[36] Seeding of the flow was accomplished using monodisperse 0.6-μm-diam spherical polystyrene latex particles.[37]

Results

In the present study the size of the ground vortex has been quantitatively determined through the use of flow visualization for varying nondimensional jet-to-ground plane spacings h/D_e, and crossflow-to-jet velocity ratios V_∞/V_j. In addition, the confining effects of varying nozzle size (i.e., varying Reynolds number) in the fixed-size tunnel test section (i.e., tunnel side wall effect) have been studied, as have the effects of the presence of the jet board through which the jet nozzle protrudes. Finally, the effects of jet nozzle exit conditions (turbulence intensity and mean velocity profile shape) have also been studied.

Nozzle Calibration

For the current work, jet exit maximum velocity has been held fixed at nominally 91.4 m/s (300 ft/s), as shown in Table 1. This yields jet Reynolds numbers based on jet diameters of approximately 5.4×10^4, 7.2×10^4, and 1.43×10^5 for the 0.95-, 1.27-, and 2.54-cm-diam nozzles. Typical traverse results for a standard uniform jet are shown in Fig. 4, whereas the annular jet results appear in Fig. 5.

To enable a rational comparison between the uniform jets and the annular jets which issue from the plugged jet nozzle, a modification of the technique developed by Ziegler and Wooler[10] has been used. Similar procedures have been used for the annular jet in hover out of ground effect by Kuhlman and Warcup.[16] Effective uniform jet velocity and diameter values are computed for an ideal top-hat velocity profile which would have the same momentum flux and initial mass flux as

Table 1 Nozzle calibration results

Nozzle type		P_{noz}, cm H_2O	q_{max}, cm H_2O	V_{max}, m/s	Q_{noz}, m^3/min	MF_{noz}, N	V_{ave}, m/s	D_{eff}, cm	V_{eff}, m/s
1.27 cm	*v*	51.64	49.45	91.91	0.6823	1.193	89.78	1.251	92.55
2*D* nozzle	*h*	51.66	49.50	92.08	0.6878	1.200	90.50	1.255	92.72
	a	51.65	49.48	91.99	0.6851	1.197	90.14	1.253	92.63
2.54 cm	*v*	50.38	48.69	91.38	2.752	4.767	90.51	2.519	92.01
2*D* nozzle	*h*	49.95	48.46	91.28	2.726	4.681	89.72	2.510	91.91
	a	50.17	48.58	91.33	2.740	4.724	90.11	2.514	91.96
0.95 cm	*v*	51.60	49.50	92.13	0.3855	0.6730	90.17	0.9390	92.78
2*D* nozzle	*h*	51.52	49.63	92.22	0.3852	0.6720	90.10	0.9382	92.87
	a	51.56	49.57	92.18	0.3854	0.6725	90.14	0.9386	92.83
1.27 cm	*v*	52.88	49.99	92.43	0.6927	1.214	91.14	1.257	93.08
screen	*h*	52.57	49.99	92.43	0.6839	1.198	89.98	1.247	93.08
	a	52.72	49.99	92.43	0.6883	1.206	90.56	1.253	93.08
1.27 cm	*v*	60.49	48.51	91.32	0.4384	0.6227	57.68	1.006	91.94
annular	*h*	59.47	49.73	92.52	0.4502	0.6493	59.24	1.013	93.17
	a	59.98	49.12	91.92	0.4443	0.6360	58.46	1.009	92.56
1.27 cm	*v*	50.83	49.05	92.13	0.6834	1.181	89.91	1.250	92.77
4*D* nozzle	*h*	51.19	49.68	92.75	0.6876	1.188	90.47	1.250	93.40
	a	51.01	49.37	92.44	0.6855	1.185	90.19	1.250	93.09
0.95 cm	*v*	52.12	52.45	94.38	0.3835	0.6826	89.71	0.9252	95.09
7*D* nozzle	*h*	52.20	53.11	94.82	0.3893	0.6922	91.05	0.9299	95.53
	a	52.16	52.78	94.60	0.3864	0.6874	90.38	0.9275	95.31
1.27 cm	*h*	50.55	49.25	92.39	0.6774	1.156	89.13	1.243	93.04
13*D* nozzle									

v—vertical; *h*—horizontal; *a*—average.

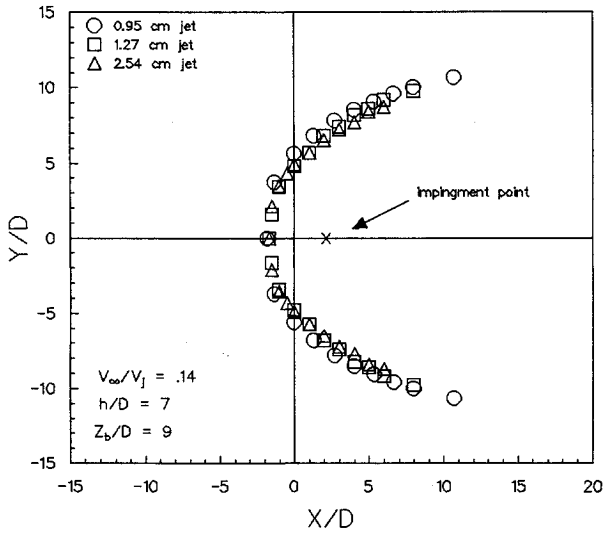

Fig. 6 Nondimensional ground vortex shape at V_∞/V_j = 0.14, h/D_e = 7.0, for all three jet diameters.

measured for the nonuniform annular jet. The effective uniform jet momentum flux is computed from

$$MF = \dot{m}\sqrt{\frac{2RTq_{max}}{p + [(\gamma - 1)/\gamma]q_{max}}} \quad (1)$$

The effective uniform jet area is computed from

$$A_e = MF/2q_{max} \quad (2)$$

from which the effective uniform jet diameter is computed as

$$D_e = \sqrt{4A_e/\pi} \quad (3)$$

Also, the effective uniform jet exit velocity is computed from

$$V_e = \dot{m}/\rho A_e \quad (4)$$

It should be noted that for the standard nozzles the effective velocities and diameters computed in this fashion are nearly equal to the measured centerline velocities and the physical nozzle exit diameters (Table 1). Furthermore, for the nonuniform annular jet, the value of V_e computed is again close to the measured maximum velocity, while D_e is slightly larger than the diameter of a circular nozzle with an area equal to the annular flow area between the nozzle wall and the cylindrical centerbody or plug. The present technique for computing effective jet diameter and velocity has been shown to be equivalent to Ziegler and Wooler's original method.[34] Also, it has been noted[18] that this procedure is identical at low Mach number to the dimensional reasoning of forming jet length and velocity scales from Q and $K = \int u^2\, dA$, where $V_e = K/Q$ and $A_e = Q^2/K$. For the nonuniform annular jet results, the velocity ratio has been computed using V_e. Jet spacing from the nozzle exit to the ground plane h/D_e has also been adjusted to match the value for the uniform jet. Comparisons of ground vortex size have been made by nondimensionalizing all dimensions by D_e. Since D_e for the annular jet is smaller than for the uniform jets, this has the effect of enlarging the measured ground vortex for the annular jet and moving it towards the uniform jet ground vortex.

Flow Visualization—Standard Nozzles

Flow visualization data for the case of V_∞/V_j = 0.14 and h/D_e = 7 was obtained for the three different standard nozzle sizes, and the resulting nondimensional shape of the ground vortex is shown in Fig. 6. A very small discrepancy can be seen for the 0.95-cm-diam case, possibly indicating that there is some blockage for the two larger nozzles caused by the large volume flow rates of the larger jets in the crossflow channel formed by the ground board, tunnel sidewalls, and the jet board. The data does in general, however, appear to have good nondimensional agreement. To examine a case with a smaller h/D_e and larger ground vortex, the three different diameter nozzles were utilized to study a frequently studied case of h/D_e = 3 at several velocity ratios. Figure 7 shows the nondimensional shape of the ground vortex for V_∞/V_j = 0.125. Again, the data has good nondimensional agreement near the centerline, but the side walls of the tunnel cause some blockage for the case of the 2.54-cm jet, as noticed

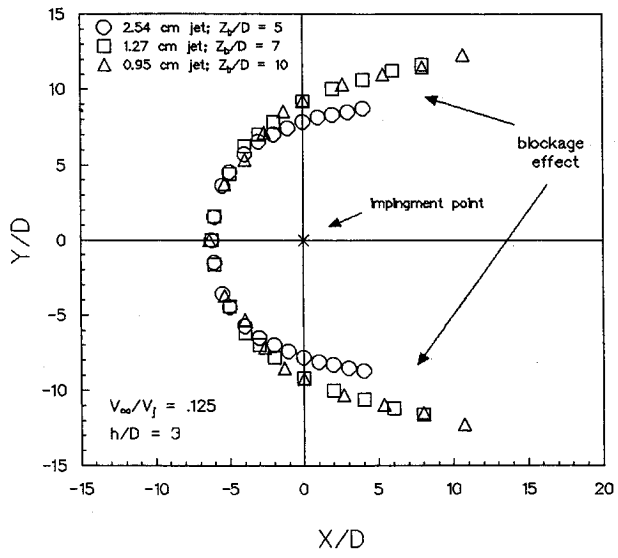

Fig. 7 Nondimensional ground vortex shape at $V_\infty/V_j = 0.125$, $h/D_e = 3$, for all three jet diameters.

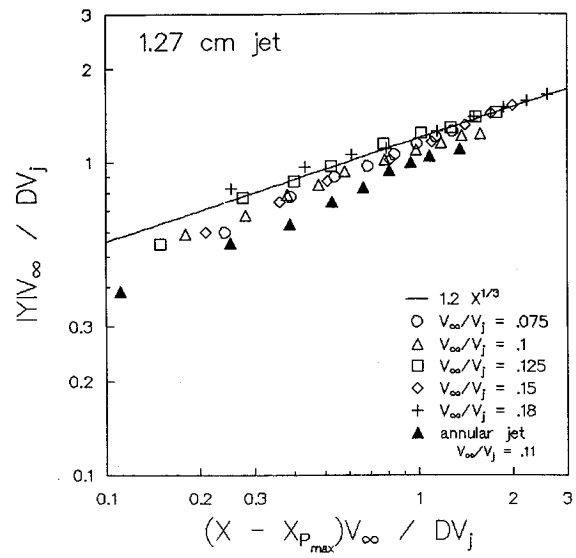

Fig. 10 Collapse of ground vortex shape data when rescaled by V_∞/V_j; 1.27-cm-diam nozzle, $h/D_e = 3$.

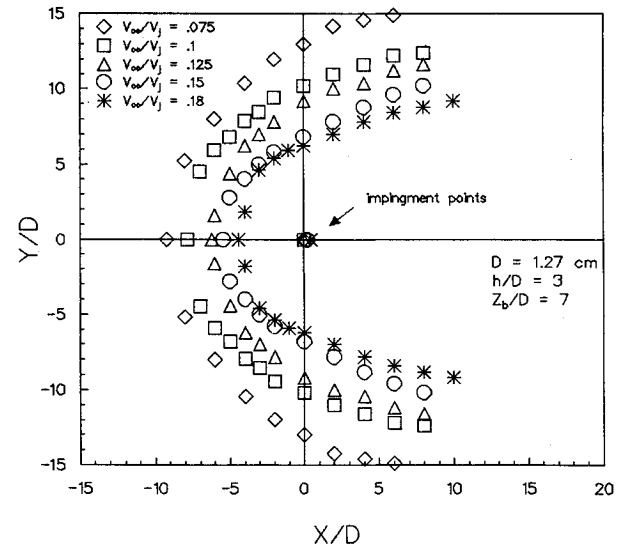

Fig. 8 Nondimensional ground vortex shape at $h/D_e = 3$ for 1.27-cm-diam jet for various crossflow-to-jet velocity ratios.

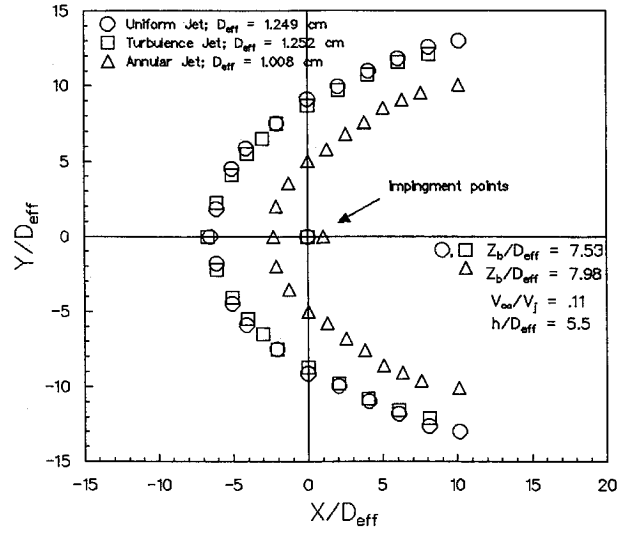

Fig. 11 Nondimensional ground vortex shape at $V_\infty/V_j = 0.11$, $h/D_e = 5.5$ for three different nozzle types.

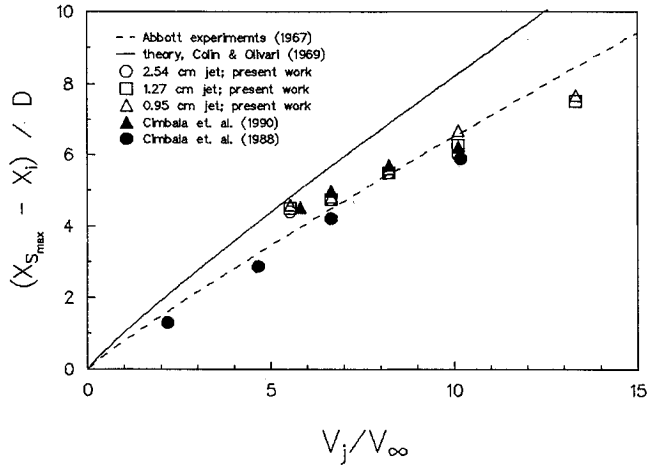

Fig. 9 Nondimensional upstream separation of ground vortex vs V_j/V_∞.

by the decreased lateral extent of the ground vortex. For the ground vortex formed by the 2.54-cm jet, the sides of the ground vortex pass within 4 or 5 diam of the tunnel side walls, causing the deflection observed in the graph. Similar results at several other velocity ratios indicate no significant blockage effects for all three jet nozzles for velocity ratios of 0.15 or larger.[34] The ground vortex shape for the 1.27-cm-diam jet at $h/D_e = 3$ is plotted for several V_∞/V_j values in Fig. 8.

The maximum upstream penetration of the ground vortex, located at y/D_e equal to zero, has been examined extensively by Cimbala et al.[26] The upstream penetration (nondimensionalized by jet diameter) of the ground vortex for various V_j/V_∞ at $h/D_e = 3$ has been presented in Fig. 9. For this figure, upstream penetration has been taken as the difference in the separation point at $y/D_e = 0$, and the jet impingement point at $y/D_e = 0$. For most velocity ratios (<0.125), the impingement point is essentially located at $x = 0$. The impingement point was easily determined from the flow visualization as a result of the formation of a radial wall jet oil flow which formed when the fog fluid smoke would condense on the ground board. The present data agree well with the 3-in.-jet data of Cimbala et al., and with moving model results due to

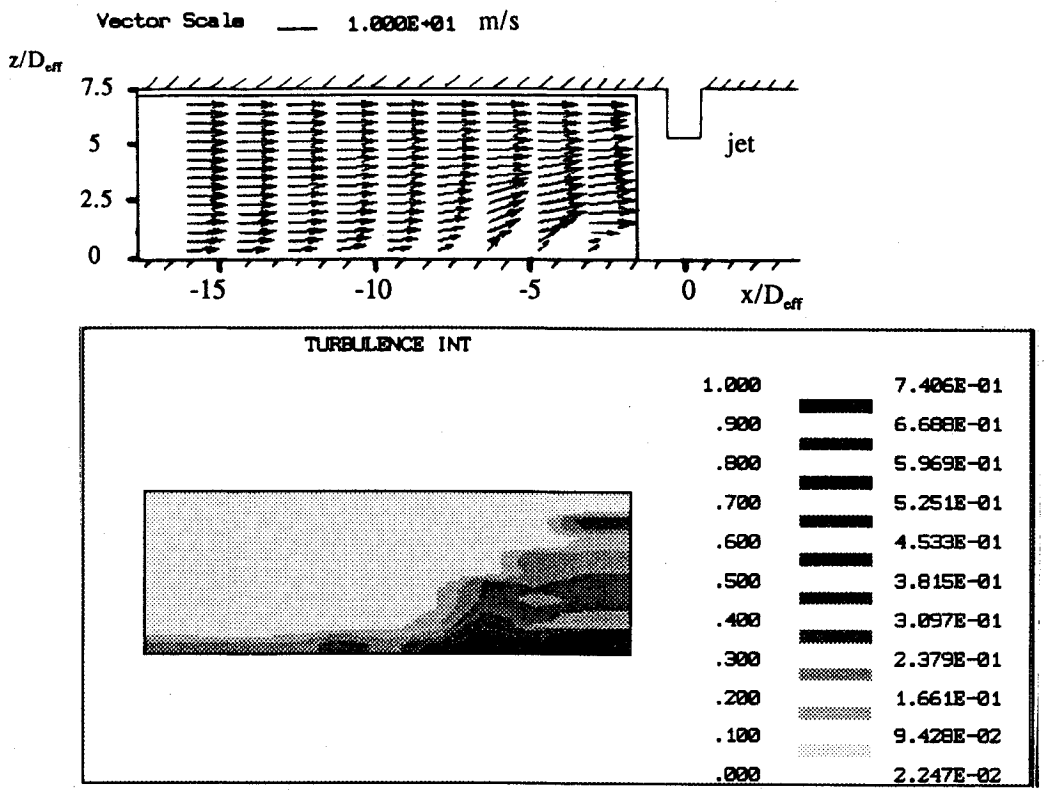

Fig. 12 Mean velocity vectors and turbulence intensity contours on centerline upstream of jet nozzle; LV data at $V_\infty/V_j = 0.11$, $h/D_e = 5.5$.

Abbott.[5] Results of Colin and Olivari[7] do not agree as well with the present work. However, the present upstream penetration data match a curve-fit equation from Colin and Oliveri

$$x_p/D = C(V_j/V_\infty)^{0.9} \tag{5}$$

with the constant adjusted to $C = 0.7$.

The ground vortex shape data presented in Fig. 8 have been approximately collapsed to a single curve in Fig. 10, where nondimensional distances have been multiplied by V_∞/V_j, and x has been measured from the point of maximum upstream penetration of the ground vortex. Using logarithmic axes, the ground vortex shape data cluster around a line with a slope of one-third. Scatter in y coordinate at a fixed x is about $\pm 10\%$. The shape of this curve, $y \sim x^{0.33}$, has also been found to closely match a different ground vortex shape equation due to Colin and Olivari,[7] which was developed based on a potential flow model using the stagnation streamline for the two-dimensional Rankine half-body.[34] Both of these curve fit equations for ground vortex shape use the centerline upstream penetration x_p to define the zero for the x coordinate, where x_p is given by the curve fit given by Eq. (5) in the previous paragraph. Thus, for example, the present equation for ground vortex shape is

$$yV_\infty/(DV_j) = 1.2[(x - x_p)V_\infty/(DV_j)]^{1/3} \tag{6}$$

The effect of the ground board spacing on the ground vortex size was also examined. Cimbala et al.[25] observed a significant difference in ground vortex behavior if the jet board location Z_b/D_e was equal to the h/D_e of the nozzle (no nozzle length). They also observed that a value of Z_b/D_e equal to two diameters greater than h/D_e was the limiting case for the jet board to influence the ground vortex size or shape. For the case of $h/D_e = 4.34$, and $V_\infty/V_j = 0.11$, Z_b/D_e has been varied as 6.34, 8.34, and 17.34, (nozzle lengths of 2, 4, and 13 diam, respectively); as well as a case where Z_b/D_e was 17.34 and most of the jet board had been removed, leaving only the 4-in.-wide center piece to confine the ground vortex in the vertical direction (z). Results of this study have been given by Cavage.[34] A very slight difference was seen in ground vortex shape, as well as upstream penetration, for the two cases where the $Z_b/D_e = 17.34$ compared to the two cases with smaller Z_b/D_e values. This indicates that the presence of a jet board would tend to alter the ground vortex shape for nozzle lengths as large as 4 diam, but only by a very small amount.

Flow Visualization—Nonstandard Nozzles

The three different 1.27-cm-diam nozzle configurations have been compared for the case of $V_\infty/V_j = 0.11$, $h/D_e = 5.5$ as shown in Fig. 11. The jet effective diameters have been calculated by the method similar to Ziegler and Wooler[10] as described above. Ground vortex sizes have been nondimensionalized by D_e to allow for a rational comparison of ground vortex shape and size. The ground vortex formed by the turbulence screen nozzle was the same size as the ground vortex formed by the standard nozzle, to within experimental uncertainty. This indicates that increased jet turbulence intensity (nominally 3–4%, vs less than 1% for the standard nozzle, as measured with a hot wire anemometer) did not significantly alter the size of the ground vortex.

On the other hand, the annular nozzle configuration resulted in a significant reduction in ground vortex size. The ground vortex formed by the plugged nozzle has a very similar shape to that formed by the standard nozzle, but has a completely different upstream penetration at all equivalent y/D_e locations. The annular jet which is formed by the plug in the nozzle has been shown to have a significant change in the decay rate of the jet in the near field.[18] This is due to an increase in entrainment, due to the formation of a wake shear layer within the jet flow itself, as well as the increased surface area of the jet shear layer relative to the jet effective diameter. This quicker jet decay and increased entrainment significantly reduces the observed ground vortex size, most likely by reducing the effective value of V_j/V_∞.

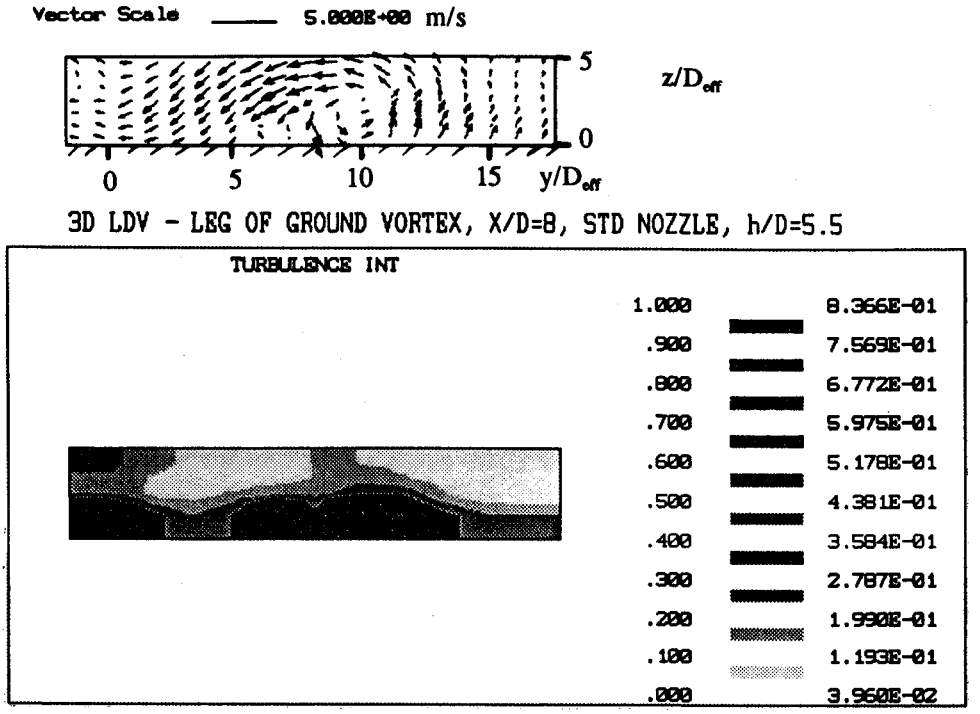

Fig. 13 Mean velocity vectors and turbulence intensity contours in y-z plane at $x/D = 8$; LV data at $V_\infty/V_j = 0.11$, $h/D_e = 5.5$.

LV Data

Three-component LV data have been obtained on the centerline upstream of the jet nozzle for the standard $D = 1.27$ cm uniform velocity nozzle at $V_\infty/V_j = 0.11$, $h/D_e = 5.5$. This is the same uniform jet configuration which has been compared with the annular jet in Fig. 11. Mean velocity vectors in this centerline plane of symmetry have been plotted in Fig. 12. Also shown are contours of turbulence intensity level. Spanwise mean velocities across the symmetry plane were measured to be small (less than 5% of the mean axial velocity). Acceleration and upwards deflection of the crossflow by the ground vortex are clearly visible. Since only slight decelerations are observed near the ground plane, it may be concluded that the approach boundary layer is no more than $0.4D_e$ in thickness. Data in the ground vortex itself is somewhat sparse. This is due to some problems in adequately seeding the ground vortex from upstream in the tunnel plenum. The present seeding technique using an alcohol-water mixture and an atomizing nozzle to inject the 0.6-μm polystyrene latex particles caused a recondensed fog to form in the jet impingement region, and to a lesser extent in the ground vortex itself. Also, when this technique was used to seed the jet, no particles were observed in the jet. It is expected that seeding the jet with dry solid particles using a fluidized bed feeder would eliminate this problem. Also, no data have been obtained in the jet itself in the present work, again because of this difficulty in seeding the jet. Measured turbulence intensities in the ground vortex are quite high, approaching 80%, although turbulent intensity in the freestream ahead of the ground vortex was no more than 2%. The measured location of the ground vortex is consistent with flow visualization studies. The velocity data time records have not been analyzed spectrally to explore whether the large observed unsteadiness in the ground vortex is broadband or comprised of relatively few peaks. However, velocity histograms in the ground vortex have been observed to be quite broad, with no indication of any multiple peaks as would be expected if the flow at a point were simply switching back and forth between two different relatively steady states. Figure 13 presents the LV mean velocity data for this same uniform jet configuration in a y-z (crossflow) plane, at $x = 8D_e$ downstream of the jet axis. Again, measured turbulence intensity contours have also been shown. Here the ground vortex is clearly visible even though only the freestream flow has been seeded; however, this vortex is relatively weak. Rotational mean velocities in the y-z plane are no more than approximately 25% of the freestream axial velocity. Again, unsteady turbulent velocities are as high as 80% of the mean velocity in the ground vortex. The axial velocity is reduced in the center of the ground vortex at this x location,[34] indicating that this flow originates from very near the ground plane. The observed lateral extent of the ground vortex of approximately $13D_e$ is consistent with flow visualization results in Fig. 11. The present LV results are qualitatively similar to two-component LV data presented by Cimbala et al.[26]

Conclusions

The interaction of a single axisymmetric jet with a ground plane in the presence of a weak crossflow has been investigated, primarily through the use of flow visualization, to study the formation of the ground vortex ahead of the jet impingement point. This study has been motivated by jet VTOL and STOL aircraft applications.

Changing the jet nozzle size at fixed h/D_e and V_∞/V_j has been found to have a relatively small effect on the nondimensional size of the ground vortex in the present study, at least for $V_\infty/V_j \geq 0.15$. This variation of the jet diameter simultaneously altered jet Reynolds number, since V_j was held fixed, and altered the nondimensional location of the tunnel sidewalls.

Furthermore, for the present facility, where the jet nozzle protrudes at least $2D$ beyond the jet board, it has been found that moving the jet board further away from the ground plane, while holding the jet exit-to-ground plane spacing h/D_e fixed, causes only very minor changes in ground vortex behavior.

Variation of ground vortex size and shape and jet impingement point with crossflow-to-jet velocity ratio V_∞/V_j has been found to follow trends documented by previous investigations. As V_∞/V_j increases from 0.075 to 0.180, both upstream penetration of the ground vortex and jet impingement location are swept downstream, and the ground vortex becomes narrower. Two different simple equations have been found to predict the present ground vortex shape results, primarily at

$h/D_e = 3$, in terms of the maximum upstream penetration, to an accuracy of $\pm 10\%$.

Increasing jet exit turbulence level from below 1%, to between 3–4%, was observed to have a negligible effect on ground vortex size. This is not surprising, since interaction of the jet with the ground plane and crossflow should be expected to greatly alter velocities and to efficiently generate turbulence in the ground vortex. However, the nonuniform annular jet mean velocity profile was shown to reduce the size of the ground vortex region by 30–50% compared to an equivalent uniform jet having equal momentum and mass fluxes. The annular jet has been shown previously to lead to enhanced jet decay rate, width growth, and entrainment relative to the uniform jet, and to increase jet-induced lift losses in hover, while reducing such losses in crossflow out of ground effect. The present magnitude of ground vortex size reduction was consistent with the levels of entrainment increase and lift loss reduction previously observed out of ground effect for the annular jet. These results again point out the need for correct simulation of jet decay characteristics for any experimental *or* computational studies of aeropropulsion interaction. Furthermore, it would appear that the annular jet results might point towards a means of controlling ground vortex size somewhat. However, it may be that increased entrainment of the annular jet would lead to increased lift loss in spite of the reduced ground vortex size.

LV data are consistent with the flow visualization results, and indicate turbulence levels as high as 80% in the ground vortex both on the centerline and downstream of the impingement point.

Acknowledgments

The present study has been supported by the NASA Langley Research Center under Grant NAG-1-1245, Guy T. Kemmerly and John W. Paulson Jr., technical monitors.

References

[1]Margason, R. J., "Review of Propulsion-Induced Effects on Aerodynamics of Jet/STOL Aircraft," NASA TN D-5617, Feb. 1970.

[2]Margason, R. J., "Propulsion-Induced Effects Caused by Out-of-Ground Effects," Society of Automotive Engineers International Powered Lift Conf., SAE Paper 872307, Santa Clara, CA, Dec. 1987.

[3]Kuhn, R. E., "Ground Effects on V/STOL and STOL Aircraft-A Survey," AIAA Paper 85-4033, Oct. 1985.

[4]Stewart, V. R., "The Characteristics of the Ground Vortex and its Effect on the Aerodynamics of the STOL Configuration," *Proceedings of 1987 Ground Vortex Workshop*, 1988, pp. 1–38 (NASA CP 10008).

[5]Abbott, W. A., "Studies of Flow Fields Created by Vertical and Inclined Jets when Stationary or Moving over a Horizontal Surface," British Aeronautical Research Council C. P. 911, 1967.

[6]Hall, G. R., "Recirculation and Ingestion Characteristics of a Large-Scale VTOL Lift Engine Pod," NASA CR-72410, Aug. 1968.

[7]Colin, P. E., and Olivari, D., "The Impingement of a Circular Jet Normal to a Flat Surface with and Without a Cross Flow," Von Kármán Inst. Final Technical Rept., Jan. 1969, available through U.S. Defense Technical Information Center, TR AD 688953.

[8]Hall, G. R., and Rogers, K. H., "Recirculation Effects Produced by a Pair of Heated Jets Impinging on a Ground Plane," NASA CR-1307, May 1969.

[9]Margason, R. J., "The Path of a Jet Directed at Large Angles to a Subsonic Free Stream," NASA TN D-4919, Nov. 1968.

[10]Ziegler, H., and Wooler, P. T., "Analysis of Stratified and Closely Spaced Jets Exhausting into a Cross Flow," NASA CR-132297, Nov. 1973.

[11]Chassaing, P., George, J., Claria, A., and Sananes, F., "Physical Characteristics of Subsonic Jets in a Cross-Stream," *Journal of Fluid Mechanics*, Vol. 62, Pt. 1, 1974, pp. 41–64.

[12]Kuhlman, J. M., and Warcup, R. W., "Effects of Jet Decay Rate on Jet-Induced Loads on a Flat Plate," *Journal of Aircraft*, Vol. 15, No. 5, 1978, pp. 293–297.

[13]Kuhlman, J. M., Ousterhout, D. S., and Warcup, R. W., "Experimental Investigation of Effect of Jet Decay Rate on Jet-Induced Pressures on a Flat Plate," NASA CR-2979, April 1978a.

[14]Kuhlman, J. M., Ousterhout, D. S., and Warcup, R. W., "Experimental Investigation of Effects of Jet Decay Rate on Jet-Induced Pressures on a Flat Plate: Tabulated Data," NASA CR-158990, Nov. 1978b.

[15]Gentry, G. L., and Margason, R. J., "Jet-Induced Lift Losses on VTOL Configurations Hovering In and Out of Ground Effect," NASA TN D-3166, Feb. 1966.

[16]Kuhlman, J. M., and Warcup, R. W., "Experimental Investigation of Jet-Induced Loads on a Flat Plate in Hover Out of Ground Effect," NASA CR-159004, Feb. 1979.

[17]Kuhlman, J. M., and Warcup, R. W., "Jet Decay Rate Effects on Hover Jet-Induced Loads," *Journal of Aircraft*, Vol. 17, No. 8, 1980, pp. 605–607.

[18]Kuhlman, J. M., "Variation of Entrainment in Annular Jets," *AIAA Journal*, Vol. 25, No. 3, 1987, pp. 373–379.

[19]Kuhlman, J. M., and Gross, R. W., "Three-Component Laser Doppler Measurements in an Axisymmetric Jet," NASA CR-181908, Oct. 1989.

[20]Kuhlman, J. M., and Gross, R. W., "Three-Component Velocity Measurements in an Axisymmetric Jet Using LDA," AIAA Paper 90-1635, June 1990.

[21]Catalano, G. D., Chang, K. S., and Mathis, J. A., "Investigation of Turbulent Jet Impingement in a Confined Cross Flow," *AIAA Journal*, Vol. 27, No. 11, 1989, pp. 1530–1535.

[22]Chen, K. S., and Hwang, J. Y., "Experimental Study on the Mixing of One- and Dual-Line Heated Jets with a Cold Cross Flow in a Confined Channel," *AIAA Journal*, Vol. 29, No. 3, 1991, pp. 353–360.

[23]Barata, J. M. M., Durão, D. F. G., Heitor, M. V., and McGuirk, J. J., "Impingement of Single and Twin Turbulent Jets Through a Cross Flow," *AIAA Journal*, Vol. 29, No. 4, 1991, pp. 595–602; also AIAA Paper 88-2529, June 1988.

[24]Barata, J. M. M., "Numerical and Experimental Study of Fountain Flows Produced by Multijet Impingement on a Ground Plane," AIAA Paper 91-1806, June 1991.

[25]Cimbala, J. M., Stinebring, D. R., Treaster, A. L., Billet, M. L., and Walters, M. M., "Experimental Investigation of a Jet Impinging on a Ground Plane in the Presence of a Cross Flow," Society of Automotive Engineers International Powered Lift Conf., SAE Paper 872326, Santa Clara, CA, Dec. 1987.

[26]Cimbala, J. M., Billet, M. L., and Gaublomme, D. P., "Experiments on the Unsteady Ground Vortex," NASA CR-177566, Aug. 1990.

[27]Billet, M. L., and Cimbala, J. M., "Summary of an Experimental Investigation on the Ground Vortex," *Proceedings of 1987 Ground Vortex Workshop*, 1988, pp. 39–60 (NASA CP 10008).

[28]Paulson, J. W., Jr., and Kemmerly, G. T., "An Assessment of Ground Effects Determined by Static and Dynamic Testing Techniques," *Proceedings of 1987 Ground Vortex Workshop*, 1988, pp. 121–146 (NASA CP 10008).

[29]Kemmerly, G. T., and Paulson, J. W., Jr., "Investigation of a Moving Model Technique for Measuring Ground Effects," NASA TM 4080, Jan. 1989.

[30]Stewart, V. R., "An Experimental Investigation on the Ground Vortex Created by a Moving Jet," NASA CR-181841, July 1989.

[31]Van Dalsem, W. R., and Steger, J. L., "Numerical Investigation of a Jet in Ground Effect Using the Fortified Navier-Stokes Scheme," *Proceedings of 1987 Ground Vortex Workshop*, 1988, pp. 191–206 (NASA CP 10008).

[32]Van Dalsem, W. R., Panaras, A. G., and Steger, J. L., "Numerical Investigation of a Jet in Ground Effect with a Cross Flow," Society of Automotive Engineers International Powered Lift Conf., SAE Paper 872344, Santa Clara, CA, Dec. 1987.

[33]Smith, M. H., Chawla, K., and Van Dalsem, W. R., "Numerical Simulation of a Complete STOVL Aircraft in Ground Effect," AIAA Paper 91-3293, Sept. 1991.

[34]Cavage, W. M., "The Ground Vortex Flow Field Associated with a Jet Impinging in a Cross Flow for Uniform and Annular Turbulent Axisymmetric Jets," M.S. Thesis, Mechanical and Aerospace Engineering Dept., West Virginia Univ., Morgantown, WV, Aug. 1992; also NASA CR-4513, May 1993.

[35]Buchave, P., "Three-Component LDA Measurements," DISA Information No. 29, published by DISA Electronics, Denmark, Jan. 1984, pp. 3–9.

[36]Yanta, W. J., and Smith, R. A., "Measurements of Turbulence-Transport Properties with a Laser Doppler Velocimeter," AIAA Paper 73-169, Jan. 1973.

[37]Nichols, C. E., Jr., "Preparation of Polystyrene Microspheres for Laser Velocimetry in Wind Tunnels," NASA-TM-89163, June 1987.